Structural Chemistry
https://doi.org/10.1007/s11224-024-02326-0

RESEARCH

Synthesis, structure characterization, Hirshfeld surface analysis, and computational studies of 3-nitro-1,2,4-triazol-5-one (NTO):acridine

Nilgün Şen[1,2] · Jean-François Pons[2] · Yunus Zorlu[3] · Eleftheria Dossi[2] · Federica Persico[2] · Tracey Temple[2] · Nazife Aslan[4] · Akachai Khumsri[5]

Received: 28 February 2024 / Accepted: 9 April 2024

Abstract
To modify the physical features and extend applications of the 3-nitro-1,2,4-triazol-5-one (NTO), we synthesized NTO with acridine (ACR) at a molar ratio of 1:1, a neutralization reaction. Through altering the chemical composition, it was possible to alter physical properties such as thermal stability, free space (voids), packing coefficient, crystal density, difference in pKa of co-formers, morphology, solubility, and impact sensitivity, and detonation parameters . It appears that physical attributes could be entirely altered. Single-crystal and powder X-ray diffraction methods, infrared spectroscopy, mass spectrometry, nuclear magnetic resonance spectroscopy (^{1}H-NMR and ^{13}C-NMR), and thermal analysis were utilized to comprehensively characterize and confirm the formation of the structure of NTO:ACR. The substantial hydrogen bond interactions and planar layered structures observed between the cations and anions generated a complex 3D network, providing insight into the structure–property interrelationship. One intriguing feature discovered is the layered structure present in NTO:ACR, which may be responsible for the low impact sensitivity. According to the experimental results, NTO:ACR showed good thermal stability (Td = 229 °C) and outstanding impact sensitivity (IS = 100 J). Detonation velocity and pressure were calculated using the EXPLO5 software program and found to be 7006 m·s^{-1} and 20.02 GPa, respectively.

Keywords Energetic salts · 3-Nitro-1,2,4-triazol-5-one · Acridine · Non-covalent interactions · NTO

Introduction

Energetic materials (EMs), including explosives, propellants, and pyrotechnics, are described as those that produce a substantial quantity of heat and/or gaseous products being stimulated by heat, impact, shock, spark, and so on. EMs are widely employed in military and civilian applications including weapons, mining, quarrying, demolition, emergency signaling, breathing device, vehicle safety, space exploration, and entertainment [1–3]. Significant efforts are being made to create high-performance EMs that have not merely outstanding in their combustion and detonation properties, high densities, and positive oxygen balances but have also good thermal stability, sensitivity to external forces, low-cost synthesis, safe handling, and good environmental compatibility [4–7]. Despite an almost 1200-year existence, they have gradually progressed in terms of detonation power as a basic feature. For instance, during the previous century, the detonation velocity of TNT (2,4,6-trinitrotoluene), HMX (1,3,5,7-tetranitro-1,3,5,7-tetrazocane), and CL-20 (hexanitrohexaazaisowurtzitane) has increased by just 30% [8–13]. The challenge of balancing high detonation performance with low sensitivity is difficult since the energy and sensitivity of explosives frequently conflict [14–17]. Instead of

✉ Nilgün Şen
nilgunsen2001@gmail.com; nilgun.sen@pa.edu.tr

1 Institute of Forensic Sciences, Turkish National Police Academy, Ankara, Türkiye

2 Centre for Defence Chemistry, Cranfield University, Shrivenham SN6 8LA, UK

3 Department of Chemistry, Gebze Technical University, 41400 Gebze, Kocaeli, Türkiye

4 Department of Chemistry, Polatlı Science and Arts Faculty, Ankara Hacı Bayram Veli University, Ankara, Türkiye

5 School of Chemistry, University of Edinburgh, Edinburgh EH9 3FJ, UK

Published online: 30 April 2024

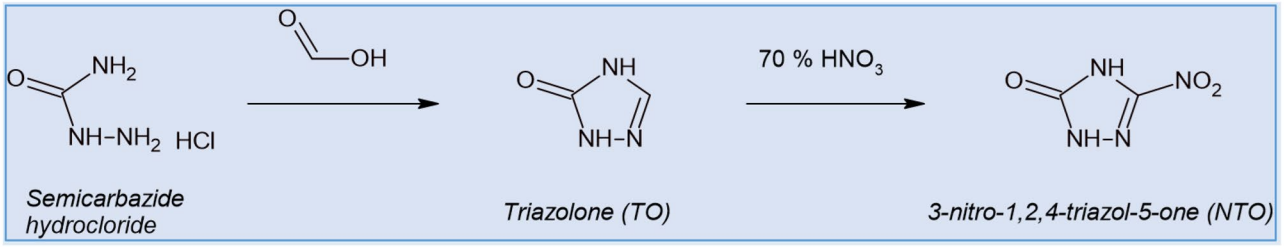

Scheme 1 NTO synthesis process

focusing solely on high energy, we can attempt to maximize the utilization of current compounds or develop new ones with remarkable, all-encompassing qualities.

3-Nitro-1,2,4-triazol-5-one (NTO) is a heterocyclic carbonyl insensitive munition that was discovered in 1905, but its explosive characteristics were not studied until the 1980s [18]. It has a higher margin of safety against unanticipated stimulus reactions and outstanding physical qualities [19–22]. It exhibits energetic performance features comparable to those of currently used secondary explosives and has the potential to be used as an explosive and propellant ingredient [23]. This compound has been demonstrated to be less hazardous to human health than conventional explosives [24, 25]. Nevertheless, this nitrogen heterocyclic energetic molecule has numerous limitations that limit its future applications, especially negative enthalpy of formation and slightly acidic nature (pKa 3.67) [26, 27]. Furthermore, because of NTO's extreme solubility in water, it is likely to be found in substantial concentrations in effluent, depending on the formulation. In rats, NTO has a high LD_{50} relative to other EMs of around 5000 mg•kg^{-1}, and investigations of water toxicity studies have yielded comparable results, with toxicity levels so low that NTO might be categorized as non-toxic [28–30]. Nevertheless, at amounts greater than 100 mg•L^{-1}, NTO contamination of the water supply causes noticeable coloration, which can lead to environmental harm by perception as it displays a bright yellow tinge to water even if no ecotoxicological impact is shown [31].

To address these problems, researchers took two basic strategies: the initial one corresponds to the acidity of NTO-derivative salts, and the second relates to the development of NTO co-crystals. The first is the well-known technique, in which numerous metal and amine salts, as well as other NTO compounds, have been and continue to be made. The second new strategy, co-crystallization, might pave the road for the use of NTO. Co-crystallization is a prominent approach to enhancing the solubility, bioavailability, and physical and chemical stability of pharmaceuticals without affecting their chemical structure [32–35]. As a unique technology, co-crystals are composed of two or more components that are found together by hydrogen bonds, π-π stacking, van der Waals forces, and halogen bonds [36–38]. Co-crystallization is used to enhance the physicochemical features and energetic performance of the composition for certain applications [39–42]. Different NTO co-crystals and salts have lately been studied theoretically and experimentally [19, 43–47]. It is demonstrated that this technology allows for the modification of physicochemical parameters and the creation of improved co-crystals with enhanced features at the molecular level. ACR, an important nitrogen-containing heterocyclic systems, acting as a weak base ($pK_b = 5.4$ in water) [48], and its salt display modest detonation performance. It may mitigate the acidity of NTO to some extent by co-crystallizing with mildly basic ACR, without consuming less energy and giving NTO an enhanced integrated performance.

The research disclosed in this paper aims to investigate a concept that has an opportunity to step change for the control of the properties of EMs, leading in safer and more effective performance. The lack of structure–property relationships presents a challenge for the design of new NTO-based co-crystals and salts. This research thereby intends to exploit the concepts of crystal engineering and co-crystallization as applied to selected energetic materials in order to accomplish the following objectives: (i) develop an enhanced understanding of how structure influences key properties, (ii) control the sensitivity of existing, and (iii) identify new EM with improved energetic properties.

Experimental section

Chemicals and preparation of the sample

Sigma-Aldrich supplied sulfuric acid (H_2SO4, 95–97%), semicarbazide hydrochloride (CH_6ClN_3O), formic acid (CH_2O_2, 85%), nitric acid (HNO_3, 70%), and ACR ($C_{13}H_9N$, 97%). NTO was synthesized in two processes, beginning with the synthesis of TO (1,2,4-triazol-5-one). It was synthesized by the reaction of semicarbazide hydrochloride with formic acid and nitrated with 70% HNO_3 (Scheme 1) [49].

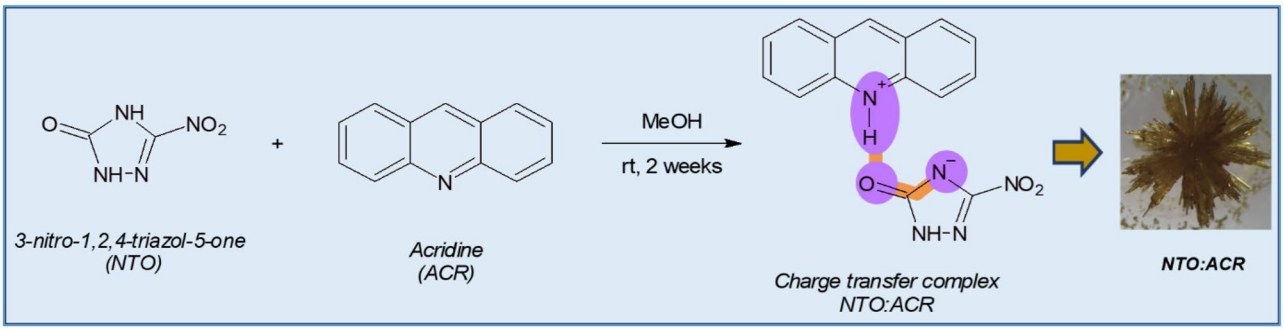

Scheme 2 Crystal formation mechanism of the NTO:ACR

NTO was verified using nuclear magnetic resonance and infrared spectroscopy (Figs. S1–S6).

Crystallization was accomplished by dissolving an equimolar ratio of NTO (46 mg) with ACR (90 mg) in methanol (about 5–10 mL) at 50 °C and for 30 min (Scheme 2).

Characterization techniques

Optical microscopy

Optical micrographs of the NTO, ACR, and NTO:ACR were examined using an Olympus BX51 microscope.e

Single crystal X-ray diffraction (SCXRD)

The measurements were carried out with a Bruker APEX II CCD three-circle diffractometer with MoKα ($\lambda = 0.71073$) radiation. APEX2 was used to index the data (Bruker. APEX2, Ver. 2014.11–0, Bruker AXS Inc., Madison, WI 2014). SAINT was used for data integration and reduction (SAINT, version 8.34A, Bruker, Bruker AXS Inc., Madison, W. No. Title, 2013). SADABS' multi-scan approach was used to adjust absorption (SADABS, version2014/5, Bruker, Bruker AXS Inc., Madison, W. No Title. 2014). NTO:ACR structure was solved by SHELXT [50] in Olex2 Software Package [51], then refined by full-matrix least-squares refinements on *F2* using the SHELXL [52]. Additional crystallographic data with CCDC reference number **2253569** for NTO:ACR has been deposited within the Cambridge Crystallographic Data Centre via www.ccdc.cam.ac.uk/deposit.

Powder X-ray diffraction (PXRD)

PXRD patterns were obtained using the Bruker D8Advance using Cu-Kα radiation ($\lambda = 1.54439$ Å) and an operating voltage and current of 40 kV and 40 mA, respectively. The temperatures ranged from 5 to 80°.

Nuclear magnetic resonance spectroscopy (NMR) spectral studies

^{1}H-NMR characterization of ACR, NTOm and NTO:ACR was obtained using a Bruker Ascend 400 MHz spectrometer with a BBFO probe, and the spectra were recorded at ambient temperature in dimethyl sulfoxide (DMSO-d_6) (typical solution of 10 mg/mL). The solvent peaks were referenced to DMSO-d_6 (2.50 ppm). Peak multiplicities were described as follows: singlet (s), triplet (t), broad triplet (brt), doublet of triplet (dt), and multiplet (m).

Infrared (IR) spectroscopy

The IR spectra were obtained with a Bruker Equinox55 with ATR equipment (wavenumber range 4000–400 cm^{-1}, resolution 4 cm^{-1}).

Differential scanning calorimetry (DSC)

Thermal characterization was performed on the materials using a Mettler Toledo LF1100 TGA/DSC 3+ equipped with a DSC sensor and operated by Stare System software v15.00 (build 8992). The tests were carried out in an inert atmosphere (N_2 flowing at 50 cm^3 min^{-1}) and at one heating rate: 10 °C min^{-1} over a range of 25–400 °C.

Mass spectrometry (MS)

Mass spectra were attained by an X500 QTOF mass spectrometer system equipped with a direct inlet (DI) unit and an electron impact ionizer. And the data was analyzed with Bruker Compass Data Analysis systems.

pH measurement

Thermo Scientific™ Orion™ 720Aplus and pH/mV/ISE Benchtop Meters were used to measure pH values of NTO, ACR, and NTO:ACR .W pH values were measured with

combined glass pH electrode and found to be 3.48, 5.34, and 4.28, respectively (Fig. S7).

Impact sensitivity measurement test

The impact sensitivity was measured using a BAM fall hammer (BFH-12) and used 30-trial Bruceton method [54, 55].

Explosive performance analysis

The EXPLO5 software program was used to calculate all explosive properties presented in this work, including detonation velocity, pressure, and oxygen balance [56].

Hirshfeld surface analysis

Hirshfeld surface and 2D fingerprint calculations were carried out on crystal structures imported from CIF files using Crystal Explorer software version 3.1 [57].

Theoretical calculations

Calculation of heat of formation (HOF)

In this study, ab initio calculations were performed using the program package Gaussian 09 (Revision-D.01) [58] and visualized with GaussView 5.0.8 [59]. SCXRD data was used to initial input data. For those computations, the hybrid B3LYP density functional with the def2-TVZP basis set in the gas phase was applied. Enthalpy values in the gas and solid phases were calculated using the complete basis set method (CBS-4 M; M refers to the method of using minimum population localization).

Non-covalent interactions (NCIs)

The NCI index is an excellent tool for studying noncovalent interactions. It has been frequently used to investigate hydrogen, halogen, and pi-pi stacking interactions [60, 61]. The basic density gradients were calculated using Multiwfn software (v.3.8) [62]. These gradients were then used for generating the demonstration graphs using the VMD (Visual Molecular Dynamics) program (v.1.9.3) [63].

Results and discussion

The outcomes of the experiments

The microscope images of NTO, ACR, and NTO:ACR

The microscope images of the NTO, ACR, and the NTO:ACR are presented in Fig. 1. The morphological distinctions between them are obvious. With the comparison of NTO and ACR, it came to light that the NTO:ACR was a yellow prism-like clear crystal with a well-defined morphology. The crystal shapes and colors are distinct from those of their co-formers (NTO in Fig. 1a, ACR in Fig. 1b, NTO:ACR in Fig. 1c).

Characterization of the NTO:ACR

SCXRD analysis A new energetic compound, NTO:ACR crystals, which are appropriate for SCXRD analysis measurements, was attained by the slow solvent evaporation method. NTO:ACR was acquired in high yields and stable in an open atmosphere under ambient conditions. The compound (NTO:ACR) SCXRD analysis was performed by choosing good-quality crystals of sufficient size ($0.15 \times 0.13 \times 0.12$ mm^3). Table S1 summarizes the crystallographic data attained and the structural refinement consequences of NTO:ACR. The ORTEP drawing and crystal structure of NTO:ACR are indicated in Fig. 2A and B. NTO:ACR forms crystals in the triclinic crystal system and corresponds to the *P*-1 space group with four molecules (Fig. 2C). Four of the two molecules per unit cell have face-to-face connection, and each side is stacked with another molecule to form an edge-to-edge configuration (Fig. 2D). In line with our design concept, the significant to building a layer-by-layer structure in EMs is strategically opt for H-bond donor–acceptor units. The acridinium cation is the hydrogen bond donor, while NTO is the acceptor. The

a **b** **c**

Fig. 1 Microscope images of NTO (**a**), ACR (**b**), and NTO:ACR (**c**)

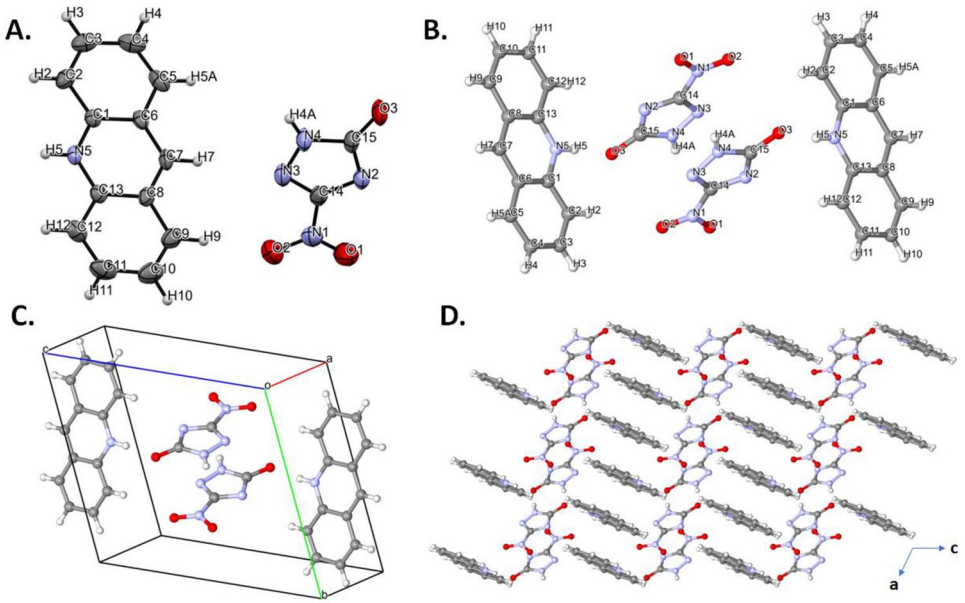

Fig. 2 ORTEP drawing of **A** NTO:ACR. **B** Crystal structure of NTO:ACR. **C** Structure of NTO:ACR in unit cell. **D** Packing diagram in the unit cell of NTO:ACR

deprotonation of NTO and protonation of ACR result in a hydrogen bond between the carbonyl of NTO and the N of the acridine ($N^+ \ldots H^- \ldots O$).

With the introduction of one hydrogen to the ACR, it altered the planer structure of the NTO precursor (Fig. 2D). The heterodimers are held together to create a molecular layer. Given the rising quantity of eutectic molecules identified through this technology, co-crystallization to get compounds with unique characteristics has been intensively investigated. NTO act as anions and ACR (N-base) as cation (Fig. 3). The presence of a (mildly) basic nitrogen of ACR helps forming the interactions seen, in particular the hydrogen bonding network. This is not surprising since the pK_a of NTO is ~ 3.7 and the pK_a for ACR is ~ 5.4 [48]. It has two ionizable hydrogen sites, which are crucial for salt formation; also, it is soluble in water, making it excellent for evaporative crystallization. Furthermore, it is nitrogen-rich and contains functional groups that are favorable for interactions such as hydrogen bonding. For acid–base complexes whose ΔpKa values lie between −1 and 4, a linear relationship between the possibility of salt formation and their ΔpKa value has been established. This relationship has enabled us to quantify prior formulations of the pKa rule, and it can be a useful tool for scientists involved in co-crystal design and salt selection strategies [64]. There are two moderate hydrogen bonds at the NTO:ACR (N_4-$H_{4A} \ldots O_3$ and N_5-$H_5 \ldots O_3$), which is already transferred onto the nitrogen atom (ACR) (Fig. 4B and Table 1). Other interactions in Fig. 4A are not hydrogen bonds; they should be regarded as necessary interactions that occur in the absence of stacking [65]. The formation of hydrogen bonds is a thermodynamically advantageous and exothermic reaction. Intermolecular bonds of hydrogen decrease molecular volume and vapor pressure while increasing molar mass, viscosity, thermal conductivity, dissolving power, phase transition temperatures, dielectric constant, dipole moment, and surface tension [66].

Given the nature of electrostatic interactions, these interactions are extremely weak. The π… π stacking interaction

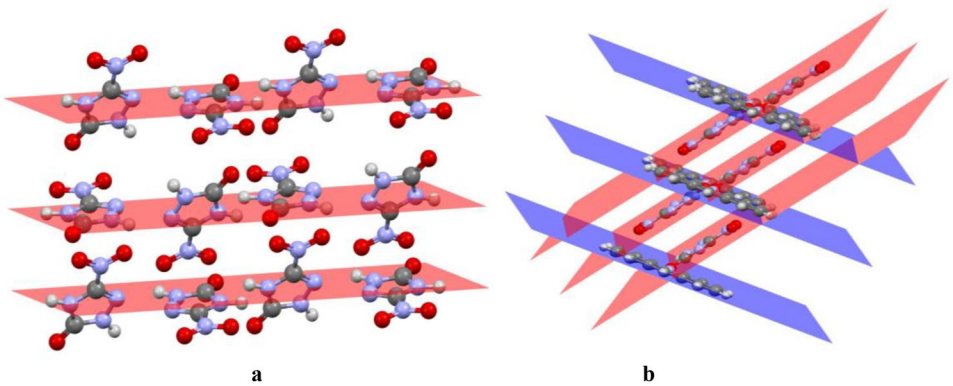

Fig. 3 Calculated planes indicating NTO stacking (**a**). Calculated planes indicating zig-zag relationship of NTO packing in NTO:ACR (**b**)

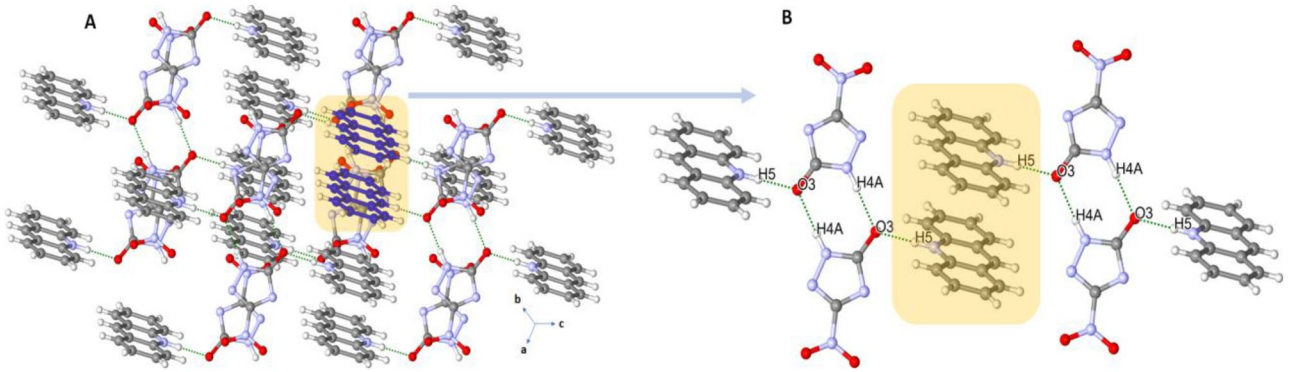

Fig. 4 The π… π stacking interaction and hydrogen-bonded pattern and in NTO:ACR

Table 1 Hydrogen bond geometries for NTO:ACR (Å, °)

D (donor)	H	A (acceptor)	[ARU][a]	D-H (Å)	H…A (Å)	D…A (Å)	D-H…A (°)
N (4)	H (4A)	O (3)	[1]	0.86	1.9	2.759 (4)	174
N (5)	H (5)	O (3)	[2]	0.86	1.75	2.606 (3)	174

[a]Translation of ARU code to CIF and equivalent position code: [1] = $-x$, $1-y$, $3-z$, [2] = x, y, $-1+z$. Note 1: analysis of potential hydrogen bonds and schemes with d (D… A) < R(D) + R(A) + 0.50, d (H… A) < R(H) + R(A)-0.12 Ang., D-H… A > 100.0 Deg. Note 2: *HBs lengths and angles are measured on Mercury 4.1.3 [47]

occurs between two parallel ACR cations (center to center distance of 3.66 Å, Fig. 4A). IR spectrum data, ^{1}H- and ^{13}C-NMR spectra, and mass spectrometry were used to further characterize and support the SCXRD analysis of NTO:ACR structure.

N–H…O interactions are seen in the IR spectrum, but some signals are shifted. The N…H bands of the NTO at 3200 cm^{-1} shift around 3300 cm^{-1}. This could also be the ACR N–H salt formation, or even an indication of the N–H…O = C hydrogen bond. Owing to formation of hydrogen bonds, stretching vibration of some signals shift about 100 cm^{-1} to the low energy levels [67].

PXRD analysis The PXRD examination confirmed the formation of NTO:ACR, and the PXRD patterns of NTO, ACR, and NTO:ACR are presented in Fig. 5. The PXRD pattern of the salt (NTO:ACR) is clearly distinct from its co-formers, identifying the NTO:ACR as a novel compound rather than product of crystal transformation.

NMR spectral studies

To confirm the type of interaction of ACR with NTO molecules, ^{1}H-NMR spectra of the single components and NTO:ACR were recorded in DMSO-d_6 solution. The ^{1}H-NMR spectrum of ACR (Fig. 7) shows all absorptions between 9.11 and 7.60 ppm; a singlet at 9.11 ppm is attributed to H-7 proton; a multiplet centered at 8.17 ppm assigned to the overlapping signals of H-2, H-2′, H-5, and H-5′; and two sets of doublets of triplets assigned to H-3 and H3′, H-4, and H-4′ (Fig. 6) at 7.86 ppm and 7.65 ppm respectively. The ^{1}H-NMR spectrum of NTO shows a singlet at 12.83 ppm attributed to the NH protons.

^{1}H-NMR spectrum of the NTO:ACR (DMSO-d_6) shows the deshielding of all ACR protons (Fig. 7, red line). In detail, the singlet attributed to H-7 is deshielded by 0.03 ppm from 9.12 to 9.15 ppm, and the multiplet assigned to H-2, H-2′, H-5, and H-5′ coalesces into a broad triplet and is deshielded by 0.02 ppm from 8.20–8.15 ppm to 8.22–8.15 ppm. The two multiplets assigned to H-3, H3′ and H-4, H-4′ are deshielded by 0.01 ppm to 7.90–7.85 ppm and by 0.02 ppm to 6.67–7.62 ppm, respectively. The small deshielding shifts observed by ^{1}H NMR support the formation of the weak acridinium-NTO salt (NTO:ACR) (Scheme 2), which is also confirmed by SCXRD analysis.

Mass spectral (MS) analysis

The base peaks correspond to the ACR and NTO compounds. It can be displayed in Fig. S8 at *m/z* 180.08 $[ACR+H]^{+}$, $[C_{13}H_{10}N_1]^{+}$ and at *m/z* 129.00 $[NTO\text{-}H]^{-}$, $[C_2H_1N_4O_3]^{-}$. MS analysis only supports the presence of the two entities (NTO and ACR).

DSC analysis

In order to estimate the thermal stabilities of NTO:ACR, DSC testing was performed. The DSC traces in Fig. 8 show

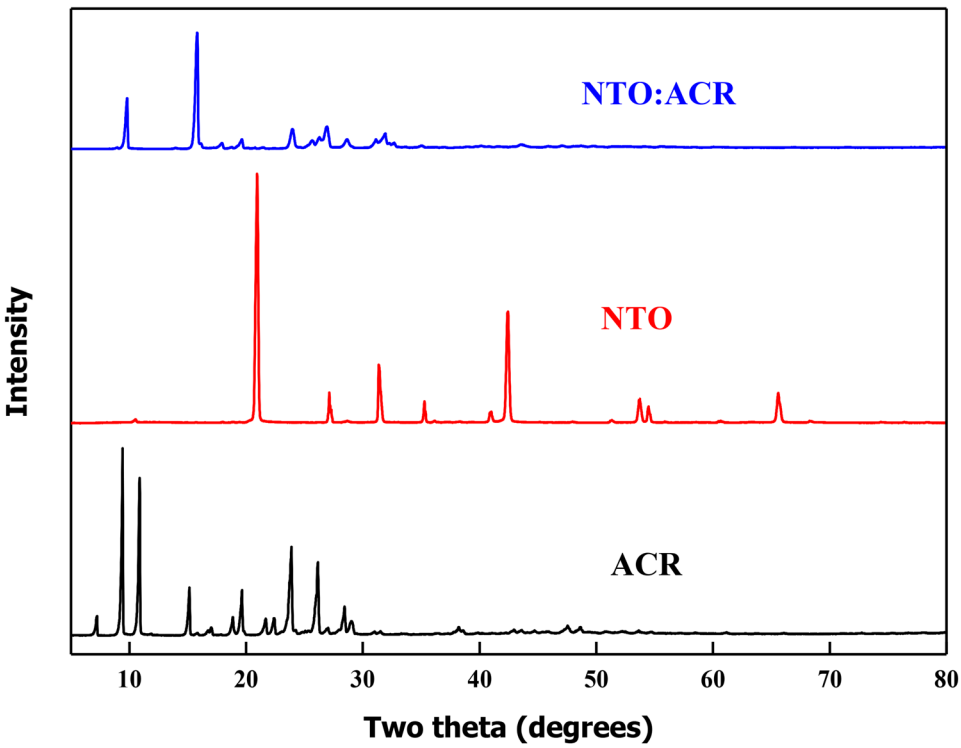

Fig. 5 PXRD patterns for ACR, NTO, and NTO:ACR

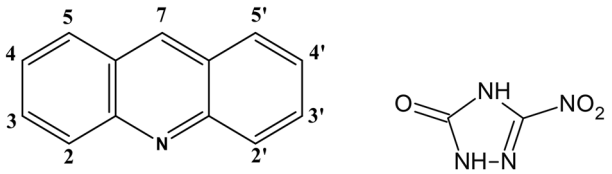

Fig. 6 Chemical structure of ACR (left) with assigned numbered carbon atoms and NTO (right)

that NTO:ACR salt shows only one exothermic peak with onset temperature 226 °C and peak maximum 229 °C. The decomposition temperature has a lower value than that of pure NTO (279 °C). The curves show that the thermal behavior of NTO:ACR differs from that of their co-formers, and the variations in thermal stability of these substances imply the formation of a new compound. The formation of new compound could lead to in intermolecular hydrogen

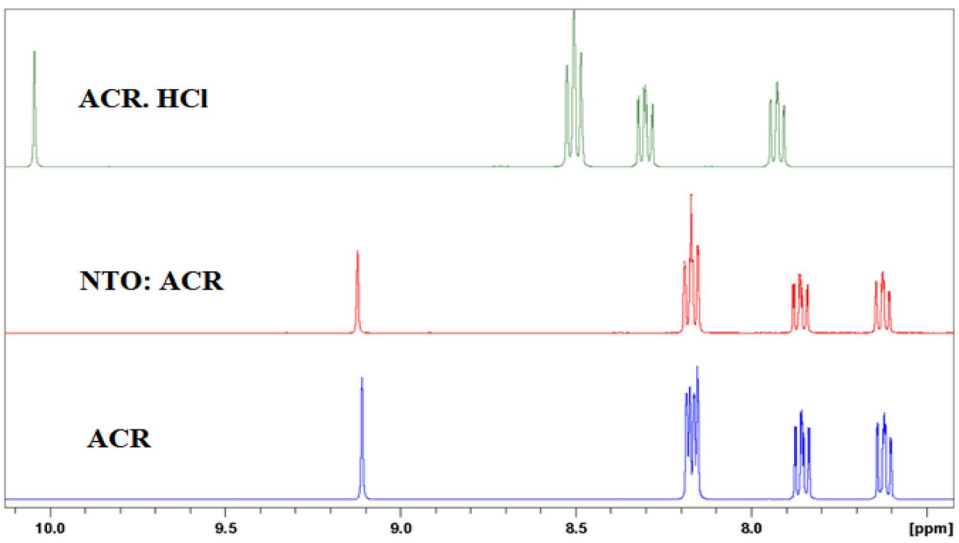

Fig. 7 ^{1}H NMR spectra of the ACR, NTO:ACR, and a ACR. HCl . **Acridinium chloride**: ^{1}H-NMR (DMSO d_6 + DCl, d) 7.93 (2H, m), 8.30 (2H, m), 8.51 (4H, brq, J = 5.45 Hz), 10.04 (1H, s). **NTO**:**ACR**: ^{1}H-NMR (DMSO d_6, d): 7.62 (1H, m), 7.86 (1H, m), 8.17 (1H, s), 9.12 (1H, s), 12.82 (1H, s). **ACR** : ^{1}H-NMR (DMSO d_6, d):7.64 (2H, m), 7.86 (2H, m), 8.17 (4H, m), 9.11 (1H, s)

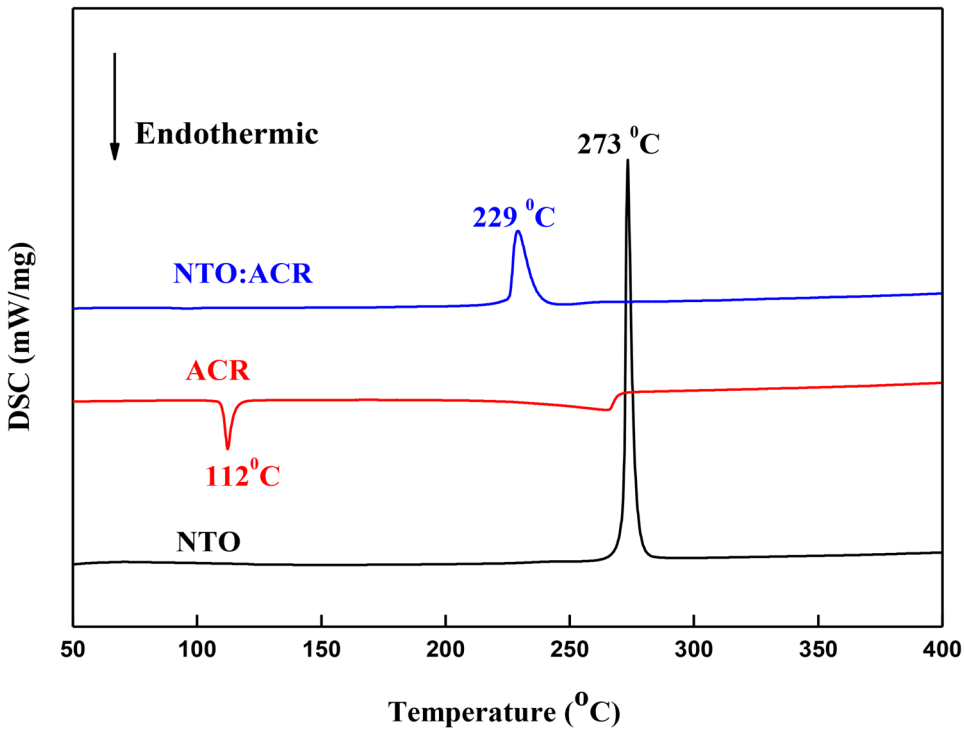

Fig. 8 Differential scanning calorimetry plots for NTO, ACR, and NTO:ACR (°C)

Table 2 The main bands of the IR spectra of NTO, ACR, and NTO:ACR (cm^{-1})

Assignment	NTO	NTO:ACR	ACR
C-H stretching aromatic vibration			3053
N–H stretching vibration	3203	3047	
C = O stretching vibration	1699	1650	1316
NO_2 asymmetric stretching vibration	1541	1591	
C–C stretching aromatic vibration		1487	1556
NO_2 symmetric stretching vibration	1346	1340	
C-N stretching vibration	1188	1047	1313
C = N stretching aromatic amine		1629	1616

bonding. Intermolecular hydrogen bonds have been found to increase thermal conductivity, resulting in greater hot spot energy transmission, dissipation, and greater insensitivity [2, 68–70].

Infrared (IR) spectroscopy analysis

The IR spectra of NTO, ACR, and NTO:ACR are indicated in Figs. S6, S9, and S10. The assignments for the most characteristic vibrational bands are listed in Table 2. It can be determined from the Table 2 that a group of low-intensity bands assigned to N–H stretching vibration of NTO decreased from the region of 3203 to 3047 cm^{-1}, while the C = O stretching of NTO shifted from the region of 1699 to 1650 cm^{-1}, and the C-N stretching vibration decreased from 1188 to 1047 cm^{-1}. At the same time, some peak shift occurs for both ACR and NTO bonds. The hydrogen bond increases the X–H bond length, causing the corresponding stretching vibration band in the IR spectrum to move towards lower frequencies [67].

Outcomes of the theoretical calculations

Hirshfeld surface (HS) analysis

Hirshfeld surface (HS) studies were carried out in order to acquire a better knowledge of the packing motifs and inputs of the key intermolecular interactions that determine the molecular design of substances. Figure 9a depicts HS projected in two orientations on the d_{norm} property. The Crystal Explorer 3.1 software program was utilized to assess the strength and relevance of hydrogen bonds along with additional intermolecular interactions, including their effect on crystal form, 2D fingerprints (FP), and the relevant HS [71]. It was conducted according with the standards outlined in the literature and the instances presented [72], demonstrating the existence of the interactions identified by Mercury software [53] and illustrated in Table 1. The color scale is utilized to differentiate the HS's various intermolecular interaction areas. The HS analyses for NTO:ACR are shown in Fig. 9a, which shows surfaces that have been mapped over d_{norm} (−0.7844 to 1.4763 Å). The consequences of the details are shown in Fig. 9a which are plainly visible in these locations, with considerable circular depressions

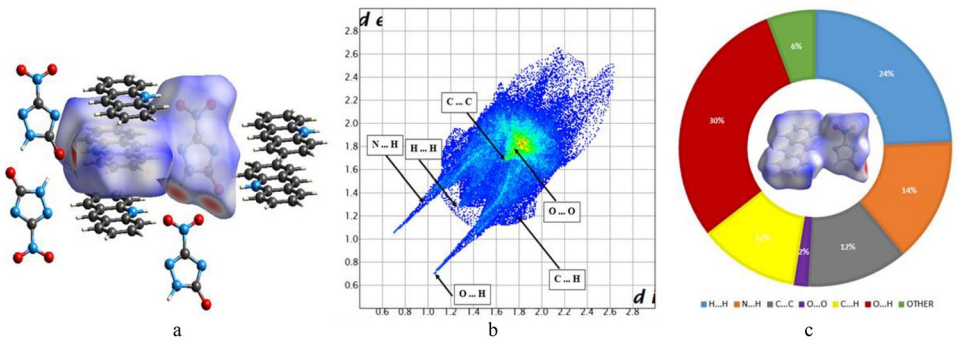

Fig. 9 **a** HS mapped with d_{norm}. **b** FP plots. **c** Populations of intermolecular and interatomic contacts of NTO:ACR

(deep red) visible on the surface, demonstrating N_4-H_{4A}…O_3 and N_5-H_5…O_3 intermolecular interactions. The red color dots in the FP plots represent short contacts for the O…H, H…H, N…H, C…H, O…O, and C…C interactions Fig. 10, emphasizing their importance in the molecular packing between NTO and ACR. The FP graphs in Fig. 9b show two separate "tails" for N–H…O, hydrogen bonds extending down to approximately $d_i = 0.75$ Å and, $d_e = 1.16$ Å for NTO:ACR. The 30% O…H, 24% H…H, and 14% N…H interactions remain the most significant contributors to total HS and can be seen as the "'idge" of the FP. The arrangement of red-blue triangles in Fig. 11b is typical of π… π stacking (ACR…ACR), showing in the FP as a characteristic value approximately $d_e = d_i = 1.8$ Å [73]. Moderate hydrogen bonds (N–H…O) were some of the most critical intermolecular interactions, as seen in Fig. 4A and B; this is dependable with the HS calculations and crystal structure data.

Theoretical calculation of heat of formation (HOF)

HOF is a significant measure for evaluating the explosive performance of EMs and can be determined using Eq. (1) [74–76], where ΔH_f°(g, M) symbolizes the enthalpy of for-

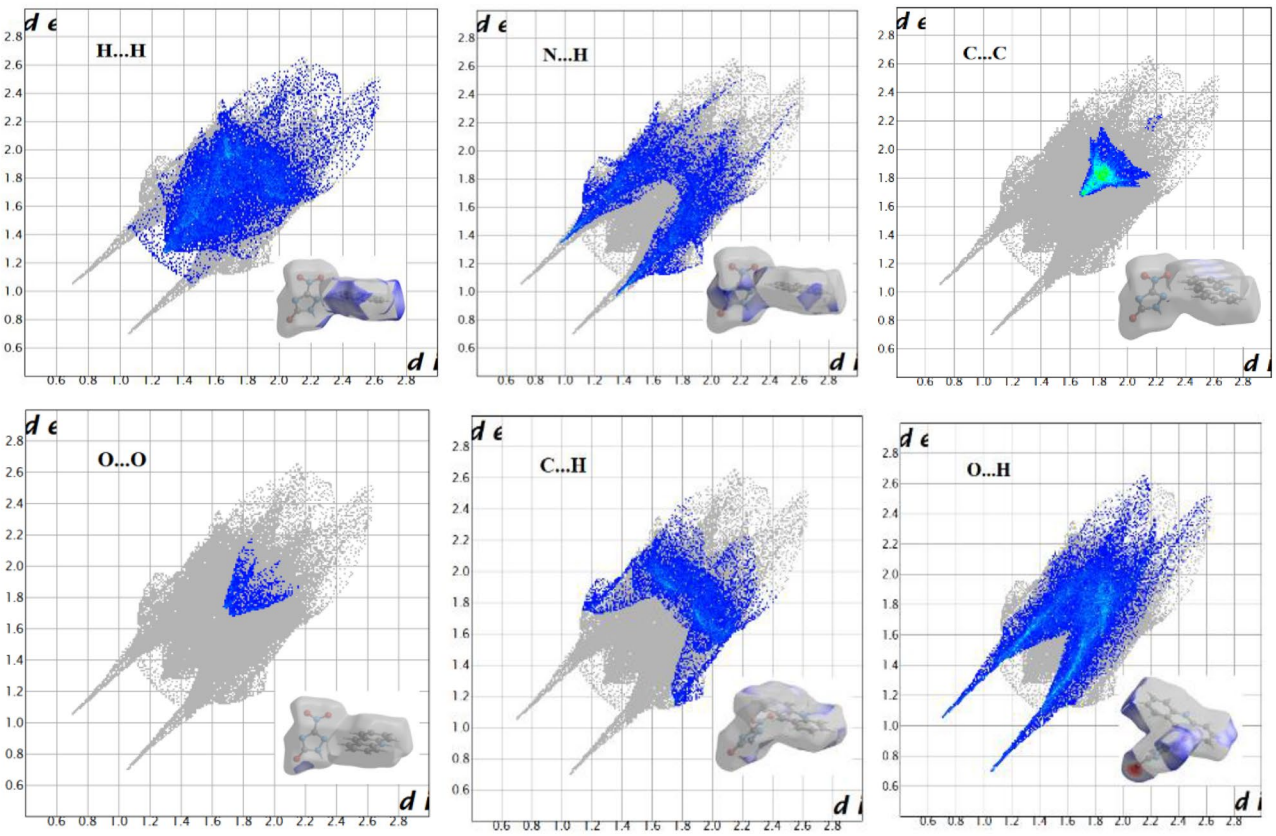

Fig. 10 FP plots for NTO:ACR, displaying contributions from various contacts

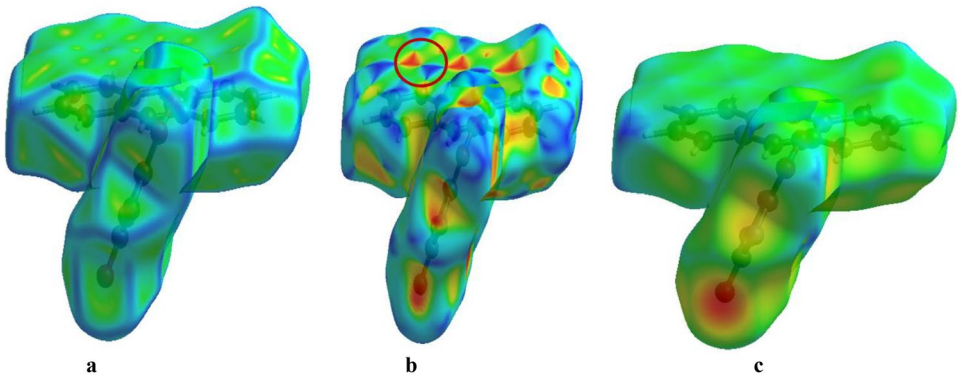

Fig. 11 **a** Curvedness, **b** shape index, and **c** d_e

Table 3 Gas-phase enthalpy of formation results

Entry	P.G.[a]	NIMAG[b]	-H^{298} (a.u.)[c]	ΔH_f°(g, M) (kJ•mol^{-1})[d]
NTO	C_1	0	519	38.00
NTO:ACR	C_1	0	1069	168.90

[a]Point group

[b]Number of imaginary frequencies

[c]Enthalpy values obtained from the CBS-4 M calculations

[d]Enthalpy of formation (in gas phase)

Table 4 Calculated ΔH_f° (sub, M), ΔH_f° (s, M), and ΔH_f° (g, M) results of NTO and NTO:ACR

Entry	Gas phase	Solid phase	
	ΔH_f° (g, M)	-ΔH_f° (s, M)	ΔH_f° (sub, M)
NTO	38	58	96
NTO:ACR	168	37	206

mation of the investigated molecule (M) in gas phase; $H^\circ_{(\text{molecule})}$ represents the calculated enthalpy value of the molecule M with the CBS-4 M method (H^{298} in Table 3); $\Sigma H^\circ_{(\text{atoms})}$ symbolizes of calculated enthalpies for the separate atoms (H, C, N, O) and $\Sigma\Delta H^\circ_{f(\text{atoms})}$ stands for experimental values of the enthalpy of formation (ΔH_f°) for the corresponding atoms H, C, N, and O to be 217, 716, 472, and 249 kJ•mol^{-1}, respectively [77].

$$\Delta H_f^\circ(\text{g, M}) = H^\circ_{(\text{molecule})} - \Sigma H^\circ_{(\text{atoms})} + \Sigma\Delta H^\circ_{f(\text{atoms})} \quad (1)$$

Furthermore, it is widely accepted that, to precisely examine the detonation properties of EMs, the calculation of the solid-phase heat of formation ΔH_f°(s, M) is necessary, and this is easily performed done by applying Hess's law (Eq. 2) [78].

$$\Delta H_f^\circ(\text{s, M}) = \Delta H_f^\circ(\text{g, M}) - \Delta H_f^\circ(\text{sub, M}) \quad (2)$$

where ΔH_f°(sub, M) indicates the heat of sublimation, which may be determined through the Rice and Politzer equation (Eq. 3) [79].

$$\Delta H_f^\circ(\text{sub, M}) = aA^2 + b(\nu\sigma^2_{\text{tot}})^{0.5} + c \quad (3)$$

where A denotes the surface area of the 0.001 electron/Bohr^3 iso-surface of the electronic density, ν represents the degree of balance between positive and negative potentials on the isosurface, and finally, σ^2_{tot} is an index of evaluating the variability of the electrostatic potential on the molecular surface (Table 4). A, ν, and σ^2_{tot} values were calculated by using Multiwfn program (v.3.8–submenu 12: quantitative analysis of molecular surface) [62]; other coefficients ($a = 2.670 \times 10^{-4}$ kcal•mol^{-1}, $b = 1.650$ kcal•mol^{-1}, and $c = 2.966$ kcal•mol^{-1}) were obtained from the literature [80].

Electrostatic potential (ESP) maps

ESP is an essentially significant physical property of compounds since it offers information on charge density distribution and chemical reactivity. In accordance with Fig. 12, positive ESP (red regions) is mainly dispersed across the main skeleton, while negative ESP (blue areas) focuses on the molecules' borders, particularly around the nitrogen and oxygen atoms, due to their higher electronegativity. The entirety of the following alterations points to variances in NTO:ACR charge dispersion which may result in changes in sensitivity.

Non-covalent interaction (NCI) plots

In order to show the intermolecular interactions of the NTO:ACR in real space, a reduced density gradient (RDG) study utilizing electron density was performed. RDG can identify non-covalent interactions (NCIs), which can provide important information on the source of molecular change, crystal packing, and stability [81, 82]. Chen et al. suggested the following relationship between the functions RDG and (r) [83].

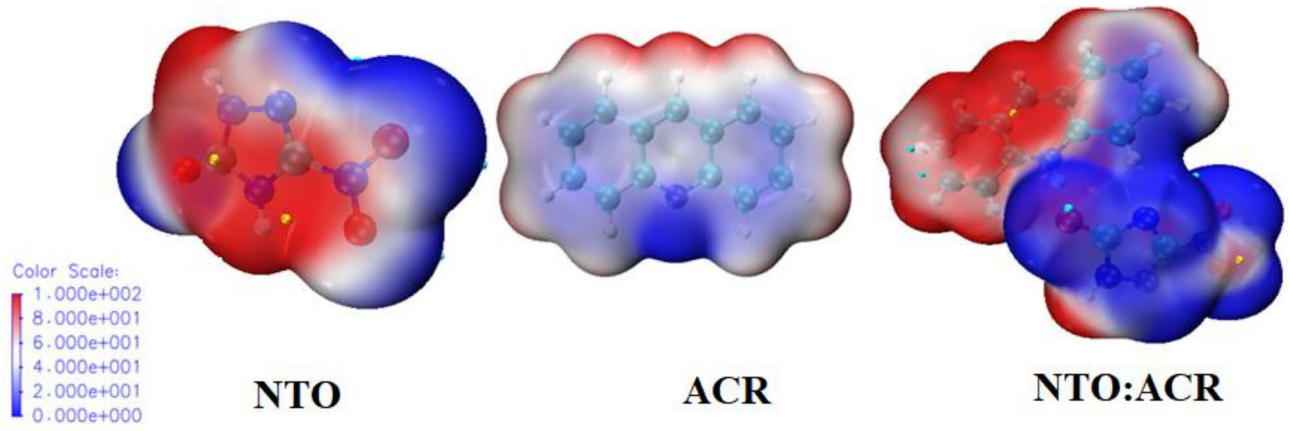

Fig. 12 ESP of NTO, ACR, and NTO:ACR

$$\mathrm{RGD} = \frac{1}{2(3\pi^2)^{1/3}} \frac{|\nabla \rho(r)|}{\rho(r)^{4/3}} \tag{4}$$

$$(\Omega) = \mathrm{sign}\big(\lambda_2(r)\big)\rho(r) \tag{5}$$

where $\rho(r)$ is the electron density, and $\mathrm{sign}(\lambda_2(r))$ is the sign of the second largest Hessian eigenvalue. The spikes are classified into three groups in RDG maps: the hydrogen bond area, the vdW interaction area, and the steric area. Initially, we investigate a case with ρ ranging from −0.04 to −0.03 a.u., which occurs within the hydrogen bond area (Fig. 13a, b). It is obvious that NTO:ACR salt is formed through intermolecular interactions including N_4-H_{4A}…O_3 and N_5-H_5…O_3. Following that, in the vdW interaction region with values ranging from −0.01 to 0.005 a.u., it is shown that NTO:ACR exhibits greater spikes, confirming significant vdW interactions (Fig. 13a, b). As shown in Fig. 13a and b, the scatter points and electron density of

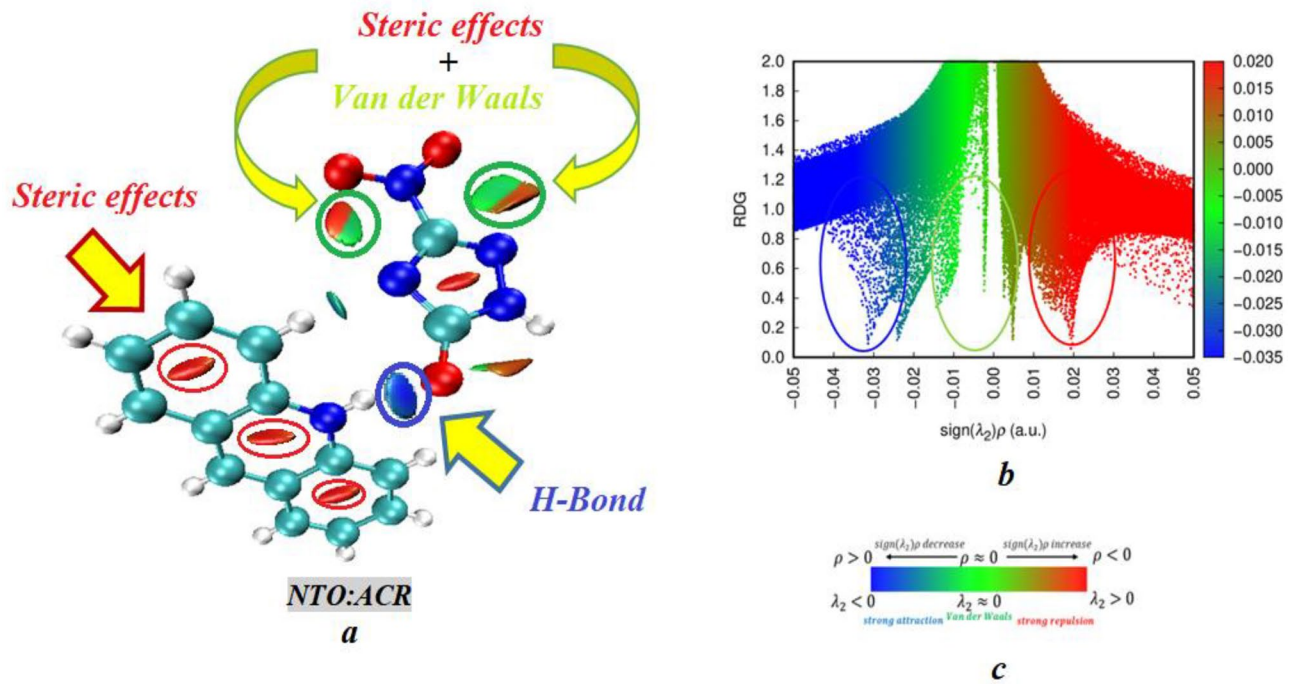

Fig. 13 RDG map and non-covalent interaction plots of low-gradient iso-surfaces for NTO:ACR

Table 5 Packing coefficient and free space of NTO and NTO:ACR

Entry	Packing coefficient (%)	Free space (voids) (%)	Impact sensitivity (J)
NTO	74.13	5.9	100
NTO:ACR	69.04	12.7	100

Table 6 Calculated detonation properties of NTO, and NTO:ACR

Entry	Ω (%)[a]	IS (J)[b]	Gas phase		Solid phase	
			D ($m \cdot s^{-1}$)[c]	P (GPa)[c]	D ($m \cdot s^{-1}$)[c]	P (GPa)[d]
NTO	−24.6	100	8747	33.01	7200	21.04
NTO:ACR	−168.1	100	7006	20.02	5480	8.75

[a]Oxygen balance

[b]Impact sensitivity was measured by BAM hammer instrument

[c]detonation velocity

[d]detonation pressure were calculated using EXPLO5 V6.04

NTO:ACR in the steric area (varying from 0.01 to 0.05 a.u) have sharper spikes and more points, confirming significant strong repulsion interactions. It is straightforward to deduce that moderate hydrogen bonds, vdW forces, and steric effects account for a significant portion of NTO:ACR intermolecular interactions.

Detonation parameters for NTO:ACR

Impact sensitivity

Impact sensitivity was executed on NTO and NTO:ACR. NTO:ACR are insensitive, with no signs of initiation up to the testing limit of 100 J (Table 5). NTO:ACR is substantially less impact sensitive than NTO, and this is attributed to the layered structure of NTO:ACR. NTO:ACR has layered structures akin to TATB (triaminotrinitrobenzene), one of the most insensitive traditional EMs.

Free space in the crystal lattice and packing coefficient

By applying Mercury CSD Ver. 4.1, the free space, i.e., voids, and packing coefficient of NTO and NTO:ACR were calculated [53]. As a consequence of the formation of NTO:ACR, the packing coefficient was altered. Despite the fact that NTO:ACR is not dense than NTO, the new compound's making drastically altered the packing coefficient and voids (Table 5) (Figs. S11 and S12). Furthermore, higher compactness indicates less free volume in the crystal, causing molecular breakdown and the occurrence of hot spots, resulting in greater insensitivity [69, 84, 85].

Calculation of detonation velocity, pressure, and oxygen balance

The characteristics of detonation are crucial for acquiring a fundamental comprehension of EM performance. The oxygen balance, detonation velocity, and pressure were calculated using EXPLO5 V6.04. It uses the Becker-Kistiakowsky-Wilson's equation of state for gaseous detonation products and Cowan-Fickett's equation of state for solid carbon [56]. The detonation parameters were calculated at the C-J point. The primary detonation products were thought to consist of C, N_2, H_2O, CH_4, NH_3, CO_2, C_2H_6, H_2, CO, CH_2O_2, C_2H_4, HCN, and CH_3OH (Figs. S13–S15). Calculated heat of formation (ΔH_f° (g, M), ΔH_f° (s, M)) and detonation parameters are listed in Table 6.

Conclusion

The co-crystallization method was utilized to form a novel energetic compound 3-nitro-1,2,4-triazol-5-one (NTO):acridine (ACR), which was then comprehensively characterized by IR spectroscopy, ^{1}H-NMR, ^{13}C-NMR spectroscopy, mass spectrometry, and DSC study. The structure attributes of NTO:ACR were investigated using SCXRD and PCXRD. Through changing the chemical composition, it was possible to alter physical properties such as thermal stability, free space (voids), packing coefficient, crystal density, difference in pKa of co-formers, morphology, solubility, and impact sensitivity, and calculated detonation parameters were also gathered and compared. It appears that it was possible to completely modify physical properties. The crystal structure and crystal packing features of NTO:ACR demonstrate that the anions and cations in this energetic compound have modest hydrogen-bond intermolecular interactions (N_4-H_{4A}…O_3 and N_5-H_5…O_3). Furthermore, Hirshfeld surface analysis and non-covalent interaction studies gave theoretical support to better investigate its structure–property relationship. The detonation velocity and

pressure of NTO:ACR were calculated with the assistance of the EXPLO5 program and found to be 7006 ms^{-1} and 20.02 GPa, respectively, slightly less than those of NTO. Although non-energetic components usually decrease the detonation velocity and pressure, they can significantly enhance the number of energetic co-crystals and salts, enabling a rich database for subsequent investigations in a data-driven or crystal engineering approach.

Supplementary Information The online version contains supplementary material available at https://doi.org/10.1007/s11224-024-02326-0.

Acknowledgements The authors would like to thank Dr Emily Arnold from Cranfield University for providing the data from the power X-Ray diffraction experiments.

Author contributions All authors contributed to the study conception and design. Nilgün Şen: conceptualisation, investigation, methodology, data curation, formal analysis, writing, editing, and funding acquisition. Jean-François Pons: investigation, methodology, data curation, formal analysis, writing, review, and editing. Yunus Zorlu: data curation and visualization. Eleftheria Dossi: investigation, methodology, data curation, formal analysis, writing, review, and editing. Federica Persico: formal analysis, writing, review, and editing. Tracey Temple: formal analysis, writing, review, and editing. Nazife Aslan: investigation, methodology, and data curation. Akachai Khumsri: data curation, formal analysis, validation, and software. All authors read and approved the final manuscript.

Funding This study was funded by the Scientific and Technological Research Council of Türkiye-TUBITAK-BIDEB 2219-International Postdoctoral Research Fellowship Program (Grant number: 1059B192100006).

Data availability No datasets were generated or analyzed during the current study.

Code availability Not applicable.

Declarations

Competing interests The authors declare no competing interests.

References

1. Thottempudi V, Yin P, Zhang J, Parrish DA, Shreeve JM (2014) 1,2,3-Triazolo[4,5,-e]furazano[3,4,-b]pyrazine 6-oxide—a fused heterocycle with a roving hydrogen forms a new class of insensitive energetic materials. Chem Eur J 20:542–548. https://doi.org/10.1002/chem.201303469
2. Gao H, Joo YH, Twamley B, Zhou Z (2011) Azole-based energetic salts. Chem Rev 111(11):7377–7436. https://doi.org/10.1021/cr200039c
3. Dippold AA, Izsák D, Klapötke TM (2013) A study of 5-(1, 2, 4-triazol-c-yl) tetrazol-1-ols: combining the benefits of different heterocycles for the design of energetic materials. Chem Eur J 19:12042–12051. https://doi.org/10.1002/chem.201301339
4. Millar RW, Hamid J, Endsor R, Swinton PF, Cooper J (2008) Selection and synthesis of energetic heterocyclic compounds suitable for use in insensitive explosive and propellant compositions. Propel Explos Pyrotech 33:66–72. https://doi.org/10.1002/prep.200800211
5. Badgujar DM, Talawar MB, Asthana SN, Mahulikar PP (2008) Advances in science and technology of modern energetic materials: an overview. J Hazard Mater 151:289–305. https://doi.org/10.1016/j.jhazmat.2007.10.039
6. Fischer D, Klapötke TM, Stierstorfer J (2014) Oxalylhydrazinium nitrate and dinitrate—efficiency meets performance. J Energ Mater 32:37–49. https://doi.org/10.1080/07370652.2012.750697
7. Hanafi S, Trache D, Abdous S, Bensalem Z, Mezroua A (2019) 5-Nitro-1, 2, 4-triazole-3-one: a review of recent advances. Chin J Ener Mater 27:326–347. https://doi.org/10.11943/CJEM2018371
8. Pagoria PF, Lee GS, Mitchell AR, Schmidt RD (2002) A review of energetic materials synthesis. Thermochim Acta 384:187–204. https://doi.org/10.1016/S0040-6031(01)00805-X
9. Sabatini JJ, Oyler KD (2016) Recent advances in the synthesis of high explosive materials. Crystals 6:1–22. https://doi.org/10.3390/cryst6010005
10. Chen J, Tang J, Xiong H, Yang H, Cheng G (2020) Combining triazole and furazan frameworks via methylene bridges for new insensitive energetic materials. Ener Mater Front 1:34–39. https://doi.org/10.1016/j.enmf.2020.07.001
11. Zheng Y, Zhao X, Qi X, Wang K, Liu T (2020) Synthesis of 5-(1H-pyrazol-1-yl)-2H-tetrazole-derived energetic salts with high thermal stability and low sensitivity. Ener Mater Front 1:83–89. https://doi.org/10.1016/j.enmf.2020.08.004
12. Yao W, Xue Y, Qian L, Yang H, Cheng G (2021) Combination of 1,2,3-triazole and 1,2,4-triazole frameworks for new high-energy and low-sensitivity compounds. Ener Mater Front. https://doi.org/10.1016/j.enmf.2021.05.002
13. Bu R, Jiao F, Liu G, Zhao J, Zhang C (2021) Categorizing and understanding energetic crystals. Cryst Growth Des 21:3–15. https://doi.org/10.1021/acs.cgd.0c01300
14. Zhang C (2018) On the energy safety contradiction of energetic materials and the strategy for developing low-sensitive high-energetic materials. Chin J Energy Mater 26:2–10. https://doi.org/10.11943/j.issn.1006-9941.2018.01.001
15. Zhang C, Jiao F, Li H (2018) Crystal engineering for creating low sensitivity and highly energetic materials. Cryst Growth Des 18:5713–5726. https://doi.org/10.1021/acs.cgd.8b00929
16. Jiao F, Xiong Y, Li H, Zhang C (2018) Alleviating the energy & safety contradiction to construct new low sensitivity and highly energetic materials through crystal engineering. Cryst Eng Comm 20:1757–1768. https://doi.org/10.1039/C7CE01993A
17. Teipel U (2005) Energetic materials: in particle processing and characterization. Wiley-VCH
18. Fawcett-Hirst W, Temple TJ, Ladyman MK, Coulon F (2021) A review of treatment methods for insensitive high explosive contaminated wastewater. Heliyon 7:e07438. https://doi.org/10.1016/j.heliyon.2021.e07438
19. Wu JT, Zhang JG, Li T, Li ZM, Zhang TL (2015) A novel cocrystal explosive NTO/TZTN with good comprehensive properties. RSC Adv 5:28354–28359. https://doi.org/10.1039/C5RA01124H
20. Migliaro FW, Rothgery EF (1993) Hydroxylammonium salts of 5-nitro-1,2,4-triazol-3-one. US Pat. no. 5274105
21. Botcher TR, Beardall DJ, Wight CA, Fan L, Burkey TJ (1996) Thermal decomposition mechanism of NTO. J Phys Chem 100:8802–8806. https://doi.org/10.1021/jp952984y
22. Zhao Y, Chen S, Jin S, Li Z, Zhang X, Wang L, Mao Y, Guo H, Li L (2017) Heat effects of NTO synthesis in nitric acid solution. J Therm Anal Calorim 128:301–310. https://doi.org/10.1007/s10973-016-5912-x
23. Pourmortazavi SM, Rahimi-Nasrabadi M, Kohsari I, Hajimirsadeghi SS (2012) Non-isothermal kinetic studies on thermal decomposition of energetic materials: KNF and NTO. J Therm Anal Calorim 110:857–863. https://doi.org/10.1007/s10973-011-1845-6

24. Sweeney LM, Phillips EA, Goodwin MR, Bannon DI (2015) Toxicokinetic model development for the insensitive munitions component 3-nitro-1,2,4-triazol-5-one. Int J Toxicol 34:408–416. https://doi.org/10.1177/1091581815589000
25. No author, (2018) 3-Nitro-1,2,4-triazol-5-one (2014). Toxicology and Industrial Health 34:8–14. https://doi.org/10.1177/0748233717719688
26. Mark N, Arthur J, Dontsova K, Brusseau M, Taylor S, Šimůnek J (2017) Column transport studies of 3-nitro-1,2,4-triazol-5-one (NTO) in soils. Chemosp 171:427–434. https://doi.org/10.1016/j.chemosphere.2016.12.067
27. Şen N, Dursun H, Hope KS, Nazir H, Acar N, Atakol O (2020) Towards low-impact-sensitivity through crystal engineering: new energetic co-crystals formed between picric acid, trinitrotoluene and 9-vinylanthracene. J Mol Struct. https://doi.org/10.1016/j.molstruc.2020.128614
28. Haley MV, Kuperman RG, Checkai RT (2009) Aquatic toxicity of 3-nitro-1,2,4-triazol-5-one. In: Report: ECBC-TR-726. US Army Center for Health Promotion and Preventative Medicine, Directorate of Toxicology
29. London JO, Smith DM (1985) A toxicological study of NTO. Los Alamos
30. O'Bryan TR, Ross RH (1988) Chemical scoring system for hazard and exposure identification. J Toxicol Environ Health 25:119–134. https://doi.org/10.1080/15287398809531193
31. Tennant M, Chew SC, Krämer T, Mai N, McAteer D, Pons JF (2019) Practical colorimetry of 3-nitro-1,2,4-triazol-5-one. Propel Explos Pyrotech 44:198–202. https://doi.org/10.1002/prep.201800239
32. Shen JP, Duan XH, Luo QP, Zhou Y, Bao Q, Ma YJ, Pei CH (2011) Preparation and characterization of a novel cocrystal explosive. Cryst Growth Des 11:1759–1765. https://doi.org/10.1021/cg1017032
33. Remenar JF, Morissette SL, Peterson ML, Moulton B, MacPhee JM, Guzm´anAlmarsson HRO (2003) Crystal engineering of novel cocrystals of a triazole drug with 1, 4-dicarboxylic acids. J Am Chem Soc 125:8456–8457. https://doi.org/10.1021/ja035776p
34. Weyna DR, Shattock T, Vishweshwar P, Zaworotko MJ (2009) Synthesis and structural characterization of cocrystals and pharmaceutical cocrystals: mechanochemistry vs slow evaporation from solution. Cryst Growth Des 9:1106–1123. https://doi.org/10.1021/cg800936d
35. Almarsson Ö, Zaworotko MJ (2004) Crystal engineering of the composition of pharmaceutical phases. Do pharmaceutical cocrystals represent a new path to improved medicines? Chem Commun. https://doi.org/10.1039/B402150A
36. Çelik GG, Dedeoglu B, Gürek AG, Zorlu Y, Ayhan MM (2023) Enhancing supramolecular assembly in bodipy derivatives: harnessing halogen bonding for cocrystal design. Cryst Growth Des 23:7285–7294. https://doi.org/10.1021/acs.cgd.3c00663
37. Schütrumpf A, Kirpi E, Bulut A, Morel FL, Ranocchiari M, Lork E, Zorlu Y, Grabowsky S, Yücesan G, Beckmann J (2015) Tetrahedral tetraphosphonic acids. new building blocks in supramolecular chemistry. Cryst Growth Des 15:4925–4931. https://doi.org/10.1021/acs.cgd.5b00811
38. Alshahateet SF (2011) Synthesis and X-ray crystallographic analysis of pharmaceutical model rac-ibuprofen cocrystal. J Chem Crystallogr 41:276–279. https://doi.org/10.1007/s10870-010-9872-x
39. Zhu W, Xiao J, Zhao F, Ji G, Ma X, Xiao H (2007) Molecular dynamics simulation of elastic properties of HMX/TATB. Acta Chim Sin 65:1223–1228
40. Wei C, Huang H, Duan X, Pei C (2011) Structures and properties prediction of HMX/TATB co-crystal. Propel Explos Pyrotech 36:416–423. https://doi.org/10.1002/prep.201000022
41. Landenberger KB, Matzger AJ (2012) Cocrystals of 1, 3, 5, 7-tetranitro-1, 3, 5, 7-tetrazacyclooctane (HMX). Cryst Growth Des 12:3603–3609. https://doi.org/10.1021/cg3004245
42. Sun T, Xiao JJ, Liu Q, Zhao F, Xiao HM (2014) A comparative study on structure, energetic and mechanical properties of a ε-CL-20/HMX cocrystal and its composite with molecular dynamics simulation. J Mater Chem A 2:13898–13904. https://doi.org/10.1039/C4TA01150C
43. Li JC, Jiao QJ, Gong YG, Wang YY, Liang T, Sun J (2018) Explosive performance of HMX/NTO co-crystal. IOP Conf Ser: Mater Sci Eng 292:012032. https://doi.org/10.1088/1757-899X/292/1/012032
44. Hope KS, Lloyd HJ, Ward D, Michalchuk AA, Pulham CR (2015) Resonant acoustic mixing and its applications to energetic materials. New Trends in Research of Energetic Materials, University of Pardubice, Pardubice, Czech Republic
45. Lloyd HJ (2017) Co-crystallisation of energetic materials-a step-change in the control of properties and performance of munitions. Dissertation of doctorate. University of Edinburgh
46. Ren YH, Zhao FQ, Yi JH, Xu KZ, Ma HX, Hu RZ, Song JR (2012) Studies on an ionic compound $(3\text{-ATz})^{+}$ $(NTO)^{-}$: crystal structure, specific heat capacity, thermal behaviors and thermal safety. J Iran Chem Soc 9:407–414. https://doi.org/10.1007/s13738-011-0051-6
47. Ma H, Song J, Hu R, Zhai G, Xu K, Wen Z (2004) Molecular structure, the quantum chemical investigation and the thermal behavior of the dimethylamine salt of 3-nitro-1,2,4-triazol-5-one, $(CH_3)_2NH_2{}^{+}C_2N_4O_3H^{-}$. J Mol Struct: THEOCHEM 678:217–222. https://doi.org/10.1016/j.theochem.2004.03.018
48. AAT Bioquest, Inc (2023) Quest Database™ pKa and pKb Reference Table. AAT Bioquest. https://www.aatbio.com/data-sets/pka-and-pkb-reference-table
49. Ledgard JB (2007) The preparatory manual of explosives, 3rd edn. Lulu Publishing, Morrisville, Washington, USA
50. Sheldrick GM (2015) SHELXT – integrated space-group and crystal-structure determination. Acta Crystallogr Sect A Found Adv 71:3–8. https://doi.org/10.1107/S2053273314026370
51. Dolomanov OV, Bourhis LJ, Gildea RJ, Howard JAK, Puschmann H (2009) OLEX2: a complete structure solution, refinement and analysis program. J Appl Crystallogr 42:339–341. https://doi.org/10.1107/S0021889808042726
52. Sheldrick GM (2015) Crystal structure refinement with SHELXL. Acta Crystallogr Sect C Struct Chem 71:3–8. https://doi.org/10.1107/S2053229614024218
53. Mercury CSD 4.1.0 (2022) (Build 235316). http://www.ccdc.cam.ac.uk/mercury/
54. Kosanke KL, Kosanke BJ, Sturman BT, Winokur RM (2012) Encyclopedic dictionary of pyrotechnics, 1st edn. J Pyrotechnics, USA
55. Fuh C, Lee J, Liaw C (2003) The design aspect of the Bruceton test for pyrotechnics sensitivity analysis. J Data Sci 1:83–101
56. Suceska M, Suceska M (2020) EXPLO5, Version 6.01; Brodarski Institute, Zagreb, Croatia, EXPLO5 Version 6.04
57. Spackman MA, Turner MJ, McKinnon JJ, Wolff SK, Grimwood DJ, Jayatilaka D, Spackman PR (2017) Crystal Explorer 17. Univ West Aust. http://hirshfeldsurface.net
58. Frisch MJ, Trucks GW, Schlegel HB, Scuseria GE, Robb MA, Cheeseman JR, Scalmani G, Barone V, Petersson GA, Nakatsuji H, Li X, Caricato M, Marenich A, Bloino J, Janesko BG, Gomperts R, Mennucci B, Hratchian HP, Ortiz JV, Izmaylov AF, Sonnenberg JL, Williams-Young D, Ding F, Lipparini F, Egidi F, Goings J, Peng B, Petrone A, Henderson T, Ranasinghe D, Zakrzewski VG, Gao J, Rega N, Zheng G, Liang W, Hada M, Ehara M, Toyota K, Fukuda R, Hasegawa J, Ishida M,

Nakajima T, Honda Y, Kitao O, Nakai H, Vreven T, Throssell K, Montgomery JA Jr, Peralta JE, Ogliaro F, Bearpark M, Heyd JJ, Brothers E, Kudin KN, Staroverov VN, Keith T, Kobayashi R, Normand J, Raghavachari K, Rendell A, Burant JC, Iyengar SS, Tomasi J, Cossi M, Millam JM, Klene M, Adamo C, Cammi R, Ochterski JW, Martin RL, Morokuma K, Farkas O, Foresman JB, Fox DJ (2016) Gaussian 09. Rev. D.01. Gaussian Inc., Wallingford, CT

59. Dennington R, Keith T, Millam J (2009) GaussView. Version 5.0.8, GaussView, Version 5.0.8
60. Jomaa L, Issaoui N, Roisnel T, Marouani H (2021) Insight into non-covalent interactions in a tetrachlorocadmate salt with promising NLO properties: experimental and computational analysis. J Mol Struct 1242:130730. https://doi.org/10.1016/j.molstruc.2021.130730
61. Tian L, Xu Y, Lin Q, Wang P, Lu M (2019) Syntheses of energetic cyclo -pentazolate salts. Chem Asian J 14:2877–2882. https://doi.org/10.1002/asia.201900776
62. Lu T, Chen F (2012) Multiwfn: a multifunctional wavefunction analyzer. J Comput Chem 33:580–592. https://doi.org/10.1002/jcc.22885
63. Humphrey W, Dalke A, Schulten K (1996) VMD: visual molecular dynamics. J Mol Graph 14:33–38. https://doi.org/10.1016/0263-7855(96)00018-5
64. Cruz Cabeza AJ (2012) Acid-base crystalline complexes and the pKa rule. Cryst Eng Comm 14:6362–6365. https://doi.org/10.1039/C2CE26055G
65. Steiner T (2002) The hydrogen bond in the solid state. Angew Chem Int Ed 41:48–76. https://doi.org/10.1002/1521-3773(20020104)41:1%3c48::AID-ANIE48%3e3.0.CO;2-U
66. Vereshchagin AL, Morozova EA (2022) Hydrogen bonding in insensitive high explosives. Russ J Appl Chem 95:1069–1084. https://doi.org/10.1134/S1070427222080018
67. Freedman HH (1961) Intramolecular H-bonds. I. A spectroscopic study of the hydrogen bond between hydroxyl and nitrogen. J Am Chem Soc 13:2900–2905
68. Klapotke TM, Mieskes F, Stierstorfer J, Weyrauther M (2016) Studies on energetic salts based on (2,4,6-trinitrophenyl) guanidine. Propel Explos Pyrotech 41:217–222. https://doi.org/10.1002/prep.201500338
69. Politzer P, Murray JS (2016) High performance, low sensitivity: conflicting or compatible? Propel Explos Pyrotech 41:414–425. https://doi.org/10.1002/prep.201500349
70. Wu Q, Pan Y, Xia X, Shao Y, Zhu W, Xiao H (2013) Theoretic design of 1,2,3,4-tetrazine-1,3-dioxide-based high-energy density compounds with oxygen balance close to zero. Struct Chem 24:1579–1590. https://doi.org/10.1007/s11224-012-0190-0
71. Spackman PR, Turner MJ, McKinnon JJ, Wolff SK, Grimwood DJ, Jayatilaka D, Spackman MA (2021) Crystal explorer: a program for Hirshfeld surface analysis, visualization and quantitative analysis of molecular crystals. J Appl Cryst 54:1006–1011. https://doi.org/10.1107/S1600576721002910
72. Panini P, Mohan TP, Gangwar U, Sankolli R, Chopra D (2013) Quantitative crystal structure analysis of 1,3,4-thiadiazole derivatives. Cryst Eng Comm 15:4549–4564. https://doi.org/10.1039/C3CE40278A
73. Bondi A (1964) Van der Waals volumes and radii. J Phys Chem 68:441–447. https://doi.org/10.1021/j100785a001P
74. Curtiss LA, Raghavachari K, Redfern PC, Pople JA (1997) Assessment of Gaussian-2 and density functional theories for the computation of enthalpies of formation. J Chem Phys 106:1063–1079. https://doi.org/10.1063/1.473182
75. Byrd EFC, Rice BM (2009) Improved prediction of heats of formation of energetic materials using quantum mechanical calculations. J Phys Chem A 113:5813–5813. https://doi.org/10.1021/jp806520b
76. Rice BM, Pai SV, Hare J (1999) Predicting heats of formation of energetic materials quantum mechanical calculations. J Com Flame 118:445–458. https://doi.org/10.1016/SOO10-2180(99)00008-5
77. Johnson RD III (2015) NIST computational chemistry comparison and benchmark data base (release 17b): NIST Standard Reference Database Number 101
78. Byrd EFC, Rice BM (2009) A comparison of methods to predict solid phase heats of formation of molecular energetic salts. J Phys Chem A 113:345–352. https://doi.org/10.1021/jp807822e
79. Politzer P, Murray JS (2011) Some perspectives on estimating detonation properties of C, H, N, O compounds. Cen Eur J Energ Mat 8:209–220
80. Jin XH, Hu BC, Jia HQ, Liu ZL, Lu CX (2014) DFT studies on two novel explosives based on the guanidine-fused bicyclic structure. Bull Korean Chem Soc 35:1043–1049. https://doi.org/10.5012/bkcs.2014.35.4.1043
81. Xie Z, Hu S, Cao X (2016) Theoretical insight into the infuence of molecular ratio on the binding energy and mechanical property of HMX/2-picoline-N-oxide co-crystal, cooperativity efect and surface electrostatic potential. Mol Phys 114:2164–2176. https://doi.org/10.1080/00268976.2016.1190038
82. Lin H, Zhu SG, Li HZ, Peng XH (2013) Structure and detonation performance of a novel HMX/LLM-105 cocrystal explosive. J Phys Org Chem 26:898–907. https://doi.org/10.1002/poc.3188
83. Chen T, Zhang Y, Guo SF, Zhao LM, Chen W, Hao GZ, Xiao L, Ke X, Jiang W (2019) Preparation and property of CL-20/BAMO-THF energetic nanocomposites. Def Tech 15:306–312. https://doi.org/10.1016/J.DT.2018.08.013
84. Johnson ER, Keinan S, Mori-Sánchez P, Contreras-García J, Cohen AJ, Yang W (2010) Revealing non-covalent interactions. J Am Chem Soc 132:6498. https://doi.org/10.1021/JA100936W
85. Xu Z, Yang H, Cheng G (2016) Studies on the synthesis and properties of polynitro compounds based on esteryl backbones. New J Chem 40:9936–9944. https://doi.org/10.1039/C6NJ02198K